

**COMPARING THE AGES OF OC AND CC CAIs.** E. T. Dunham<sup>1,2</sup>, A. Burman<sup>3</sup>, K. D. McKeegan<sup>1</sup>, M.-C. Liu<sup>1,4</sup>, N. Matsuda<sup>1</sup>, M. Telus<sup>2</sup>, S. J. Desch<sup>5</sup>. <sup>1</sup>EPSS UCLA, Los Angeles, CA, 90024, <sup>2</sup>EPS UCSC, Santa Cruz, CA 95064, <sup>3</sup>Dubai College, <sup>4</sup>Lawrence Livermore National Laboratory, Livermore, CA 94550, <sup>5</sup>SESE ASU, Tempe, AZ 85282 (email: etdunham@g.ucla.edu).

**Introduction:** Calcium-Aluminum-rich Inclusions (CAIs) are white  $\mu\text{m}$ - to cm-sized inclusions found in chondritic meteorites. They are thought to be the first solids to form in the Solar System (SS), due to their refractory nature and old ages [1]. CAIs are found within non-carbonaceous chondrites (NC) accreted in the inner SS and within carbonaceous chondrites (CC) accreted in the outer SS. However, NC CAIs are extremely rare ( $\sim 0.01$  area%) compared to CC CAIs ( $\sim 2$  area%) [2,3]. This is a conundrum because if CAIs were predominantly formed in the high-temperature ( $> 1300$  K) region close to the Sun, why are there  $\sim 200\times$  more CAIs in outer SS materials? Comparing NC and CC CAI characteristics can elucidate the mechanism(s) that transported and trapped CAIs in the outer SS while also constraining the timing of early SS dynamics. In addition, it can allow us to determine whether the hypothesis of an early-formed ( $< 1$  Ma) proto-Jupiter “opening a gap” and creating a localized pressure maximum in the disk [4] can explain the dichotomy in the relative abundance of CAIs in CC and NC chondrites [5]. In this model [5], large CAIs would be trapped by the pressure bump in the CC region and depleted in the NC region.

The two primary mechanisms of CAI transport are (1) diffusion of CAIs through the gas of the protoplanetary disk [5-8]; here small CAIs are predicted to be homogeneously distributed across the NC and CC regions. Or (2) transport of CAIs to the outer disk by winds [9]; here CAI populations in the inner and outer disks could be very different. Presumably if the first-formed CAIs are transported first and farthest by disk winds [9], this model suggests that NC and CC CAIs would have formed at different times.

Many ( $> 12,000$ ) CC CAIs have been studied, but relatively few ( $\sim 500$ ) NC CAIs have [e.g., 3]. Still fewer have been measured for isotope systematics. Here, we consider only ordinary chondrite (OC) CAIs because the petrologic type of enstatite chondrite (EC) is not quantified, making it difficult to assess the potential for CAI parent body alteration. Only two OC CAIs have previously been measured for Al-Mg [10,11], and eight for oxygen isotopes [12,13]. These CAIs record  $(^{26}\text{Al}/^{27}\text{Al})_0$  within uncertainty of the canonical value,  $5.2 \times 10^{-5}$  [14] and  $\Delta^{17}\text{O} \sim -23\%$ , similar to CC CAIs. However, more data are needed to statistically compare the two CAI populations.

In this study, we determined Al-Mg and oxygen isotope systematics of six OC CAIs from petrologic types 3.05–3.4. We compiled OC and CC CAI literature data for comparisons. Determining if NC and CC CAIs formed at the same time in a similar environment can constrain the timing and type of early Solar System processes.

**Methods:** *CAI characterization.* We used scanning electron microscopy (SEM) and electron microprobe analysis (EPMA) techniques to find and characterize 232 CAIs from OCs and ECs [3]. Here, we consider six multi-mineralic OC (3.05 to 3.4) CAIs which were possible to measure isotopically.

*SIMS oxygen isotope measurements.* We used UCLA’s Cameca IMS-1290 for all isotope analyses. Oxygen isotopes were measured first to avoid possible contamination from the oxygen primary beam during subsequent Mg isotope analyses. Polished CAI samples were measured with a  $\sim 75$  pA  $\text{Cs}^+$  beam, focused to a  $\sim 3 \times 2$   $\mu\text{m}$  spot, in multicollection mode (FC-EM-EM). Corrections for instrumental bias were made by using Burma spinel, Madagascar hibonite, San Carlos pyroxene and olivine.

*SIMS Al-Mg measurement.* An 1-2 nA  $\text{O}_3^-$  beam ( $\phi \sim 4 \times 3$   $\mu\text{m}$ ) was used to measure CAIs in multicollection mode (4 FCs). We used the same standards as for oxygen isotopes, with the addition of melilite composition glasses to characterize the instrumental mass fractionation and obtain the Al-Mg relative sensitivity factors [15]. IsoplotR [16] was used to determine Al-Mg isochrons.

**Results:** *OC CAI petrography.* The analyzed CAIs were found in MET 00526 (L/LL3.05,  $n=1$ ), MET 96515 (L3.10,  $n=2$ ), Wells (LL3.3,  $n=1$ ) and Sharps (H3.4,  $n=2$ ). Four are melilite-bearing and contain melilite + spinel  $\pm$  hibonite and two are hibonite-rich containing hibonite + spinel. They are all irregularly shaped, porous, with grain sizes  $< 10$   $\mu\text{m}$  and have an average diameter of 52  $\mu\text{m}$ . The melilite is  $\text{Åk}_{2-20}$  and the spinel FeO content ranges from 0.5–18 wt.%. Three of the CAIs have accessory nepheline or sodalite and/or FeO-rich spinel.

*Al-Mg isotope systematics.* All six CAIs recorded valid and robust isochrons when measurements of secondary minerals and FeO-rich spinel are excluded from the regression. Three of the four melilite-bearing inclusions, and both of the hibonite-rich inclusions,

recorded initial ( $^{26}\text{Al}/^{27}\text{Al}$ )<sub>0</sub> ratios within uncertainty of the canonical value. We present this data in addition to the two previously measured OC CAIs, as a kernel density estimate curve (KDE; Fig. 1) which has a mode of  $5.1 \times 10^{-5}$ .

**Oxygen isotopes.** The oxygen isotope analyses of spinel, hibonite, and melilite plot on or near the CCAM line. The spinel and hibonite have  $\Delta^{17}\text{O} \sim -13$  to  $-22\%$ , while the melilite has  $\Delta^{17}\text{O} \sim -12$  to  $-18\%$ .

**Discussion: Comparison to literature OC CAIs.**

Two OC CAIs were previously measured for Al-Mg: Semarkona (L3.00) 1805-2, a 480  $\mu\text{m}$ -long melilite + spinel + hibonite fine-grained CAI [10,13], and Quinyambic (L3.4) 6076-5-1, a 150  $\mu\text{m}$ -long, irregularly shaped melilite + spinel CAI [11]. They both record ( $^{26}\text{Al}/^{27}\text{Al}$ )<sub>0</sub> within uncertainty of canonical and are combined with our six OC CAIs to produce the NC KDE curve (Fig. 1). 1805-2 and 6076-5-1 were also measured for oxygen [9] in addition to six other OC CAIs from NWA 3358 (H3.1) [12]. Put together with our six CAIs, it appears that the L3.00 CAI contains only  $^{16}\text{O}$ -rich phases, while CAIs from 3.05 and higher types contain  $^{16}\text{O}$ -rich spinel and hibonite but relatively  $^{16}\text{O}$ -poor melilite and anorthite. This suggests that the  $^{16}\text{O}$ -poor composition of OC CAIs could be due to parent body alteration [12].

**Comparison of CC and OC CAIs:** We compiled isotopic and size information for  $\sim 350$  CC CAIs from  $\sim 65$  papers [e.g., 17]. To properly compare the two CAI populations, we selected CC (3.00-3.4) CAIs measured for Al-Mg that are  $< 500 \mu\text{m}$  (the largest OC CAI found). Therefore, no Allende CAIs or compact Type A or B CAIs are included. We did not include isotopically anomalous CAIs such as PLACs, SHIBs, or FUN or CH/CB CAIs. In total, our population consists of 70 small, mostly unmelted, and isotopically “normal” CC CAIs that are most analogous to our OC CAIs from 3.00-3.4. The OC CAIs are generally petrographically similar to the small, low petrologic-type CC CAIs: melilite-rich  $\pm$  spinel  $\pm$  hibonite  $\pm$  diopside  $\pm$  anorthite with minimal accessory secondary minerals. Small CC CAIs predominantly record canonical ( $^{26}\text{Al}/^{27}\text{Al}$ )<sub>0</sub>, like OC CAIs. About 70% of the CC CAIs and about 75% of the OC CAIs record ( $^{26}\text{Al}/^{27}\text{Al}$ )<sub>0</sub>  $\sim (4.0\text{--}5.5) \times 10^{-5}$ . The CAIs that appear younger ( $^{26}\text{Al}/^{27}\text{Al} < 4 \times 10^{-5}$ ) were likely either reset by a post-formation process or formed slightly later. This ( $^{26}\text{Al}/^{27}\text{Al}$ )<sub>0</sub> range indicates that most OC and CC CAIs formed within the first  $< 0.4$  Ma, agreeing with [14]. It is not likely that CAIs recording  $^{26}\text{Al}/^{27}\text{Al} \sim 4 \times 10^{-5}$  were reset because most are unmelted and contain minimal secondary mineralization. The most prominent KDE ( $^{26}\text{Al}/^{27}\text{Al}$ )<sub>0</sub> peak of the CC CAIs is  $4.8 \times 10^{-5}$ , likely not statistically distinct from the OC

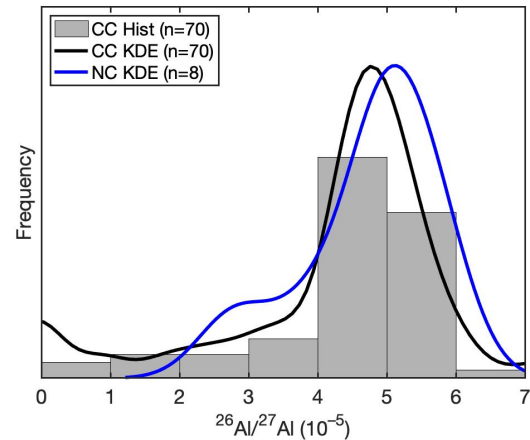


Fig. 1: Comparing small ( $< 500 \mu\text{m}$ ) NC CAI (blue) and CC CAI (black and gray)  $^{26}\text{Al}/^{27}\text{Al}$  distributions.

mode (KDE; Fig. 1). Both OC and CC CAIs tend to have  $^{16}\text{O}$ -rich spinel and hibonite, while melilite, anorthite, and pyroxene can range to  $^{16}\text{O}$ -poor compositions. Broadly, it appears that small CC and OC CAIs formed over the same time range and in a similar environment.

**Astrophysical Implications:** This data suggests that small CAIs traversing between the inner and outer Solar System likely originated from the same population, forming to 0.4 Ma, and were distributed across the NC and CC regions homogeneously. These results provide evidence that CAIs were transported outwards by diffusion through the gas.

**Acknowledgments:** This work is supported by 51 Pegasi b grant #2020-1829 (ETD). We thank Jeff Cuzzi for useful discussions.

**References:** [1] MacPherson G. J. (2014) *Treatise on Geochemistry 2<sup>nd</sup> Edition* 1.3: 139-179. [2] Scott E. R. D. and Krot A. N. (2014) *Treatise on Geochemistry 2<sup>nd</sup> Edition* 1.2: 66-137. [3] Dunham E. T., et al. (2023) *MAPS* in review. [4] Kruijer T. S., et al. (2017) *PNAS* 114:6712-6716. [5] Desch S. J., et al. (2018) *ApJ* 238:11-42. [6] Yang and Ciesla (2012) *MAPS* 47:99-119. [7] Lichtenberg et al. (2021) *Science* 371:6527. [8] Liu et al. (2022) *Sci. Adv.* 8:eabm3045. [9] Scott et al. (2018) *ApJ* 845:164-176. [10] MacPherson G. et al. (2020) *MAPS* 55: 1-20. [11] Russell S. S., et al. (1996) *Science* 273:757-762. [12] Ebert S., et al. (2020). *GCA* 282:98-112. [13] McKeegan K. D., et al. (1998) *Science* 280:414-418. [14] Jacobsen B., et al. (2008) *EPSL* 272: 353-364. [15] Dunham E. T., et al. (2020) *GGR* 12329. [16] Vermeesch P. (2018) *Geoscience Frontiers* 9: 1479-1493. [17] Davis A. M. (2022) *Annual Review of Nuclear and Particle Science* 72: 339-63. [18] Kawasaki N., et al. (2020) *GCA* 279: 1-15.